Dynamics of a single trapped ion in a high-density medium: A stochastic approach

Mateo Londoño [*] and Javier Madroñero
Centre for Bioinformatics and Photonics (CIBioFi), Universidad del Valle, Edificio E20, No. 1069, 760032 Cali, Colombia

Jesús Pérez-Ríos
Department of Physics and Astronomy, Stony Brook University, Stony Brook, New York 11794, USA

(Received 27 April 2022; accepted 7 July 2022; published 8 August 2022)

Based on the Langevin equation, a stochastic formulation is implemented to describe the dynamics of a trapped ion in a bath of ultracold atoms, including an excess of micromotion. The ion dynamics is described following a hybrid analytical-numerical approach in which the ion is treated as a classical impurity in a thermal bath. As a result, the ion energy's time evolution and distribution are derived from studying the sympathetic cooling process. Furthermore, the ion dynamics under different stochastic noise terms is also considered to gain information on the bath properties' role in the system's energy transfer processes. Finally, the results obtained from this formulation are contrasted with those obtained with a more traditional Monte Carlo approach.

DOI: 10.1103/PhysRevA.106.022803

I. INTRODUCTION

In recent years it has been possible to combine optical traps and Paul traps in a single experimental setup to obtain cold hybrid atom-ion systems [1], combining two emerging research fields: ultracold atoms and cold ions [2]. These hybrid systems are expected to incorporate the essential advantages of the two components representing a new promising scenario to study fundamental aspects of matter and light-matter interaction and to develop quantum technologies [3]. Hybrid ion-atom systems allow us to study charged-neutral interactions in a controllable way, thus revolutionizing physical chemistry and paving the way to a new field of research: cold chemistry [4]. Additionally, atom-ion hybrid systems offer a platform for studying the impurity physics of a charged particle in a neutral sea. This problem is usually approached by a many-body [5,6] or a few-body [7] perspective.

Most of the prospects and applications of hybrid atom-ion systems rely on reaching the quantum s-wave regime [3]. Ultracold atomic gases can be readily prepared in the 100-nK regime [8,9]. Then, it is necessary to use sympathetic cooling to cool down ions by bringing in contact ions with an ultracold gas (buffer gas). However, the time dependence of the electric field in Paul traps limits the temperature of the trapped ions in a buffer gas [10]. Although, using atom-ion combinations with a large mass ratio [11] such as ^{6}Li-Yb$^+$ can alleviate this effect. In general, atom-ion dynamics is studied from three different approaches: a Monte Carlo approach [12], a molecular dynamics approach [13], and a few-body *ab initio* approach [14–16]. However, there is an alternative perspective to atom-ion systems in which most of the degrees of freedom of the bath are integrated out, yielding an effective ion-bath interaction.

This work studies the dynamics of a single ion in a buffer gas from a stochastic approach. In particular, instead of considering all degrees of freedom of the bath, these are substituted by an effective stochastic force. Such a force can be modeled with different types of noise terms, which in principle allows exploring the role of the bath properties in the ion's dynamic and cooling processes via solving the Langevin equation—giving the possibility of gaining insights into the mechanisms of energy transfer between the ion and the bath. The paper is structured as follows. Section II is devoted to explaining the model based on the Langevin equation and the generalized Langevin equation (GLE) for the ion in the atomic bath, and Secs. III and IV present the main results of this formulation. In Sec. V, the more traditional hard spheres molecular dynamics methodology is introduced, and the results are contrasted with those of the stochastic formulation. Finally, Sec. VI summarizes the main results of the work and presents some perspectives.

II. LANGEVIN EQUATION MODEL

It is well-known that the motion of a single ion in a Paul trap is described by the Mathieu equation [4]

$$\frac{d^2 r_j}{dt^2} + \frac{\Omega^2}{4}[a_j + 2q_j \cos(\Omega t)]r_j = \frac{F_{\mathrm{mm},j}}{m}, \tag{1}$$

where $j = (x, y, z)$, Ω is the trap frequency, and the coefficients a_j and q_j depend on the mass of the ion and on the parameters of the trap. In particular, they are proportional to the dc and ac voltages applied to the trap, respectively, and both are inversely proportional to the distance between opposite electrodes [17]. $F_{\mathrm{mm},j}$ is the force due to possible external fields or *excess micromotion* sources, such as stray electric fields or phase differences between the ac potentials applied to the electrodes [17]. The homogeneous form of Eq. (1) admits solutions via the Floquet theorem [18]. In particular, in

[*] mateo.londono@correounivalle.edu.co

the limit of $a_j \ll q_j^2/2 \ll 1$ and making use of the adiabatic approximation, the approximate ion's position is given by

$$r_j(t) \approx A_j \cos(\omega_j t + \phi)\Big(1 + \frac{q_j}{2}\cos(\Omega t)\Big) = A_j \cos(\omega_j t + \phi) + A_j \frac{q_j}{2}\cos(\omega_j t + \phi)\cos(\Omega t),$$

where constants A_j and ϕ_j depend on the initial conditions. The adiabatic or pseudopotential approximation consists of separating the slow secular motion, driven by the secular frequency $\omega_j = \frac{\Omega}{2}\sqrt{a_j + \frac{q_j^2}{2}}$, from the fast superimposed micromotion driven by frequencies $\Omega \pm \omega_j$.

The dynamics of a trapped ion in contact with a buffer gas is more involved due to its collisions with the gas particles. In this scenario, one possible way to treat such dynamics is assuming that the ion behaves as a trapped Brownian particle in a given bath. As a result, it is possible to simulate the ion's dynamics as a Langevin stochastic process. In particular, in the case of an ion in a linear Paul trap, the degrees of freedom are decoupled, leading to the following stochastic differential equation for the motion for the jth component:

$$\frac{d^2 r_j}{dt^2} + \frac{1}{m}\int_0^t \Gamma(t-t')v_j(t')dt' + \frac{\Omega^2}{4}[a_j + 2q_j\cos(\Omega t)]r_j = \frac{F_{\mathrm{mm},j}}{m} + \frac{\zeta(t)}{m}, \tag{2}$$

where $v_j = dr_j/dt$ and the new terms in comparison to Eq. (1), $\int_0^t \Gamma(t-t')v_j(t')dt'$ and $\zeta(t)$, represent forces arising from the interaction between the ion and the bath. The former represents a friction force coming from the few-body physics of atom-ion interactions, whereas the latter represents a stochastic force.

$\zeta(t)$ is a random force resulting from the thermal fluctuations associated with the bath after integrating out most of their degrees of freedom. The random force is fully determined by its statistical properties as

$$\langle\zeta(t)\rangle = 0 \quad \text{and} \quad \langle\zeta(t)\zeta(s)\rangle = C(t-s), \tag{3}$$

where $C(t-s)$ is the force correlation function at two different times, t and s. The friction and the stochastic forces are intimately related via the fluctuation-dissipation theorem (FDT) as [19].

$$\Gamma(t-t') = \frac{1}{2k_{\mathrm{B}}T}C(t-t'), \tag{4}$$

where k_{B} is the Boltzmann constant, and T is the temperature of the bath.

In the following, we use two distinct models for the stochastic force, namely, a white noise model and a colored noise model, to study the behavior of a trapped ion interacting with an atomic bath. In addition, the results are contrasted with results from Monte Carlo simulations.

III. WHITE NOISE BATH

Assuming that the stochastic force represents a white noise, we find

$$\langle\zeta(t)\rangle = 0 \quad \text{and} \quad \langle\zeta(t)\zeta(s)\rangle = D\delta(t-s), \tag{5}$$

where $\delta(x)$ stands for the Dirac delta function of argument x, and D is the strength of the noise. Equation (5) establishes that the force at two different times is uncorrelated, and hence, the force acting on the ion only depends on the actual state of the bath. That is, a white noise leads to Markovian dynamics of the ion in a bath.

In this scenario, the FDT yields

$$\Gamma(t-t') = \frac{D}{2k_{\mathrm{B}}T}\delta(t-t'), \tag{6}$$

and the ion's dynamics is given by the following Langevin equation:

$$\frac{d^2 r_j}{dt^2} + \frac{\gamma}{m}\frac{dr_j}{dt} + \frac{\Omega^2}{4}[a_j + 2q_j\cos(\Omega_{\mathrm{RF}}t)]r_j = \frac{F_{\mathrm{mm},j}}{m} + \frac{\zeta(t)}{m}, \tag{7}$$

where we have introduced the friction coefficient defined as $\gamma = \frac{D}{2k_{\mathrm{B}}T}$.

A. Dynamics of the ion

Here, we assume a linear Paul trap configuration such that $q_x = -q_y$, $q_z = 0$, and $a_x = a_y = \frac{a_z}{2}$, satisfying $a_j \ll q_j^2/2 \ll 1$. In addition, we explicitly include the additional term $\frac{F_{\mathrm{mm},j}}{m} = \frac{eE_j}{m} = \tilde{E}_j$ ($j = x$ and y) resulting from a radial stray electric field. The few-body physics regarding atom-ion interaction is encapsulated in the diffusion coefficient, which is obtained through the Chapman-Enskog approximation [20] fed with the thermally averaged diffusion cross section, as it is described in Appendix A. Next, by virtue of the FDT, it is possible to calculate the friction coefficient from the diffusion coefficient and solve the Langevin equation, leading to the following equations for the mean position and velocity of the ion:

$$\frac{d\langle v_j\rangle}{dt} + \gamma'\langle v_j\rangle + \frac{\Omega^2}{4}[a_j + 2q_j\cos(\Omega t)]\langle r_j\rangle = \tilde{E}_j,$$
$$\frac{d\langle r_j\rangle}{dt} = \langle v_j\rangle, \tag{8}$$

where we have made $\frac{\gamma}{m} = \gamma'$ to simplify the notation. Hence, the time evolutions of the mean square values of velocity and position, and of the cross correlations, read as

$$\frac{d}{dt}\begin{pmatrix}\langle r_j^2\rangle\\ \langle v_j^2\rangle\\ \langle r_j v_i\rangle\end{pmatrix} = \mathbf{M}\begin{pmatrix}\langle r_j^2\rangle\\ \langle v_j^2\rangle\\ \langle r_j v_i\rangle\end{pmatrix} + \tilde{E}_j\begin{pmatrix}0\\ \langle v_j\rangle\\ \langle r_j\rangle\end{pmatrix}, \tag{9}$$

with $\mathbf{M}$ given by

$$\begin{pmatrix}0 & 0 & 2\\ 0 & -2\gamma' & -\frac{\Omega^2}{2}[a_j + 2q_j\cos(\Omega t)]\\ -\frac{\Omega^2}{4}[a_j + 2q_j\cos(\Omega t)] & 1 & -\gamma'\end{pmatrix}.$$

Equation (9) is solved numerically using a fourth-order Runge-Kutta method for the $j = x$ component, we use $v_x = v$ for simplicity [21], and the results are shown in Figs. 1 and 2. Figure 1 displays the time-averaged mean square position and velocity, $\overline{\langle x^2\rangle}$ and $\overline{\langle v^2\rangle}$, respectively, as a function of q_j, keeping a and Ω fixed in the absence of excess micromotion ($\tilde{E}_j = 0$). In this figure, it is noticed that the larger the value

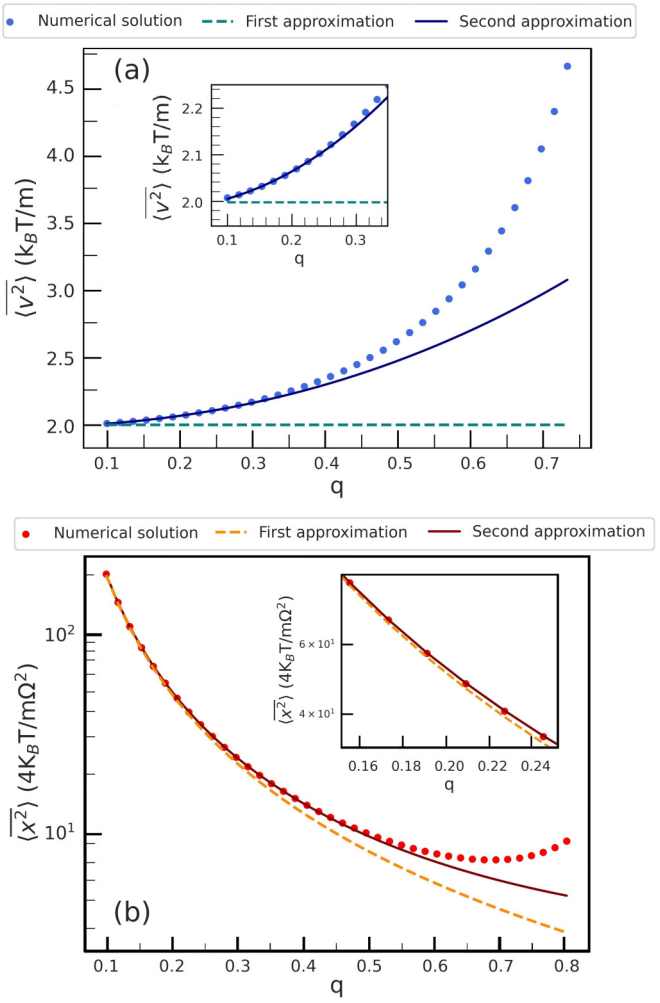

FIG. 1. Variation of the mean square x position and x velocity with respect to the $q_x = q$ parameter. The trap parameter was kept as $a = -8 \times 10^{-6}$ and $\Omega = 2\pi \times 10^6$ Hz. The points are the numerical calculations, the dashed line is the first approximation described by Eq. (13), and the solid line corresponds to the second approximation given by Eq. (15). Panels (a) and (b) show $\overline{\langle v^2\rangle}$ vs q and $\overline{\langle x^2\rangle}$ vs q, respectively. Additionally, the calculations were performed considering a $^{171}Yb^+$ ion in an ultracold cloud of ^{6}Li.

of q is, the smaller the mean square position of the ion is. On the contrary, the average square velocity of the ion increases with q. To further understand the observed behavior, we have conducted a theoretical analysis of the average mean square position and velocity of the ion based on a continued-fraction expansion following Ref. [22]. In particular, we find that $\langle r_j^2\rangle$, denoted here as σ_{rr} for simplicity, satisfies

$$\dddot{\sigma}_{rr} = -3\gamma'\ddot{\sigma}_{rr} - \left(\frac{\Omega^2}{2}[a_j + 2q_j\cos(\Omega t)] + 2\gamma'^2\right)\dot{\sigma}_{rr} - \{\gamma'\Omega^2[a_j + 2q_j\cos(\Omega t)]\}\sigma_{rr} + \frac{2D}{m} + 4\tilde{E}\gamma'\langle r_j\rangle + 4\tilde{E}\langle v_j\rangle, \tag{10}$$

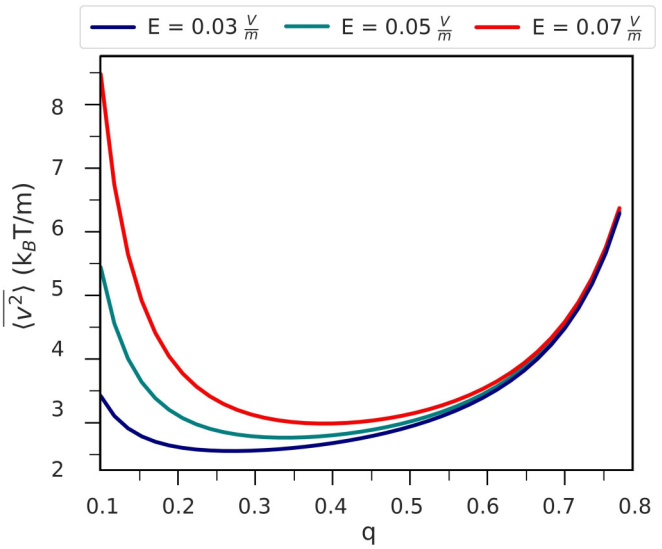

FIG. 2. Variation of the time-averaged mean square x velocity with respect to the $q_x = q$ parameter for different stray fields. The trap parameters were fixed to $a = -8 \times 10^{-6}$ and $\Omega = 2\pi \times 10^6$ Hz. The curves have been obtained numerically considering a $^{171}Yb^+$-^{6}Li mixture.

which, in the long-time regime, can be solved via the Fourier expansion method using the following ansatz:

$$\begin{pmatrix}\langle x^2\rangle\\ \langle v^2\rangle\\ \langle xv\rangle\end{pmatrix} = \begin{pmatrix}\sum_n x_n e^{-in\Omega t}\\ \sum_n v_n e^{-in\Omega t}\\ \sum_n c_n e^{-in\Omega t}\end{pmatrix}.$$

In the case of $t \gg 1/\gamma'$, i.e., a quasistationary state is reached and Eq. (10) yields

$$Q_n x_n + Q_n^- x_{n-1} + Q_n^+ x_{n+1} = 2\left(\frac{D}{m} + \frac{2\tilde{E}_x^2\gamma'}{\omega^2}\right)\delta_{n,0} + \left(\frac{\tilde{E}_x^2 q\gamma'}{\omega^2} \pm \frac{\tilde{E}_x^2 q\Omega}{\omega^2} i\right)\delta_{n,\pm1}, \tag{11}$$

with

$$Q_n = -in^3\Omega^3 - 3\gamma' n^2\Omega^2 + 2(\gamma'^2 + a\Omega^2)n\Omega i + \gamma'\Omega^2 a,$$

$$Q_n^\pm = \frac{q\Omega^2}{2}[\Omega i(2n \pm 1) + 2\gamma'].$$

In the absence of excess micromotion, Eq. (11) simplifies to $x_{n+1} = S_n^+ x_n$ for $n \geqslant 0$ and $x_{n-1} = S_n^- x_n$ for $n \leqslant 0$, with

$$S_n^\pm = -\frac{Q_{n\pm1}^\mp}{Q_{n\pm1} + Q_{n\pm1}^\pm S_{n\pm1}^\pm}. \tag{12}$$

Next, assuming $\frac{\gamma'^2}{\Omega^2} \ll 1$, the time-independent component of the Fourier expansion for the mean square position is given by

$$\overline{\langle x^2\rangle} = \frac{2D/m}{Q_0 + 2\mathrm{Re}(Q_0^+ S_0^+)} \approx \frac{k_B T}{m\omega^2}, \tag{13}$$

and the velocity and cross-correlation contributions are given by

$$v_n = (in\Omega + \gamma')c_n + \frac{\Omega^2 a}{4}x_n + \frac{\Omega^2 q}{4}(x_{n-1} + x_{n+1}),$$

$$c_n = \frac{in\Omega x_n}{2}.$$

TABLE I. Leading contributions of the Fourier expansion of the square position and velocity in the pseudopotential regime.

n	x_n	v_n
0	$\frac{k_B T}{m\omega^2}$	$\frac{k_B T}{m}$
1	$(\frac{q}{2} + \frac{q\gamma'}{2\Omega} i)x_0$	$\frac{-q\gamma'^2}{4} x_0$
2	$(\frac{3}{32}q^2 + \frac{3}{64}\frac{\gamma'}{\Omega}q^2 i)x_0$	$(-\frac{25}{184}q^2\Omega^2 + \frac{113}{368}\gamma'\Omega q^2 i)x_0$
3	$(\frac{5}{414}q^3 - \frac{181}{13248}\frac{\gamma'}{\Omega}q^3 i)x_0$	$(-\frac{1}{64}q^3\Omega^2 + \frac{3}{64}\gamma'\Omega q^3 i)x_0$

In the adiabatic limit $c_0 = \overline{\langle xv\rangle} = 0$ and hence we find

$$\overline{\langle v^2\rangle} \approx \frac{2k_B T}{m}, \tag{14}$$

leading to $\overline{\langle E_k\rangle} = \frac{1}{2}m\overline{\langle v^2\rangle} \approx k_B T$ for the spatial degrees of freedom with an rf field, which is a well-known result. The results from Eqs. (13) and (14) are shown as dashed lines in Fig. 1, where it is noticed that they can only properly describe the ion dynamics for $q \lesssim 0.1$.

Here, we go beyond previous studies by including higher-order contributions up to the third harmonic, i.e., $n = 3$, and the results are shown in Table I. We find the following time-averaged expressions for the mean square position and velocity:

$$\overline{\langle x^2\rangle} \approx \frac{k_B T}{m\omega^2}\left[\frac{1 + \frac{27}{50}q^2}{1 - \frac{1}{5}q^2}\right],$$
$$\overline{\langle v^2\rangle} \approx \frac{k_B T}{m\omega^2}\left[\frac{a\Omega^2}{4}\left(\frac{1 + \frac{14}{25}q^2}{1 - \frac{24}{31}q^2}\right) + \frac{q^2\Omega^2}{4}\left(\frac{1 + \frac{20}{25}q^2}{1 - \frac{7}{50}q^2}\right)\right], \tag{15}$$

which are displayed as the solid line in Fig. 1. As a result, the average position of the ion depends quadratically on q, whereas its kinetic energy shows a more involved behavior. The approximation given by Eq. (15) adequately describes the ion dynamics for $q \lesssim 0.3$.

In the case of a constant excess micromotion, Eq. (9) is solved numerically via a fourth-order Runge-Kutta method and the results are shown in Fig. 2, which depicts $\overline{\langle v^2\rangle}$ as a function of q_i, keeping a and Ω fixed. This figure indicates that a constant excess micromotion distorts the ion's dynamics at small values of q. On the contrary, an excess of micromotion does not alter the ion's dynamics for large values of q. Therefore, a coupling must exist between q and the excess micromotion. In particular, Eqs. (13) and (14) transform into

$$\overline{\langle x^2\rangle} = \frac{2|Q_1|^2\left(\frac{D}{m} + 2\frac{\tilde{E}_x^2}{\omega^2}\gamma'\right) - \frac{\tilde{E}_x^2 q}{\omega^2}\mathrm{Re}[Q_0^+ Q_{-1}(1+i)]}{Q_0|Q_1|^2 - \mathrm{Re}(Q_0^+ Q_1^- Q_{-1})}$$
$$\approx \frac{k_B T}{m\omega^2} + \frac{\tilde{E}_x^2}{\omega^4},$$
$$\overline{\langle v^2\rangle} \approx \frac{2k_B T}{m} + \frac{\tilde{E}_x^2}{\omega^2}, \tag{16}$$

establishing a quadratic dependence of the mean square velocity of the ion on the applied electric field, as it is corroborated in Fig. 3. This figure displays the dependence of $\overline{\langle v^2\rangle}$ concerning the constant external field, comparing numerical results

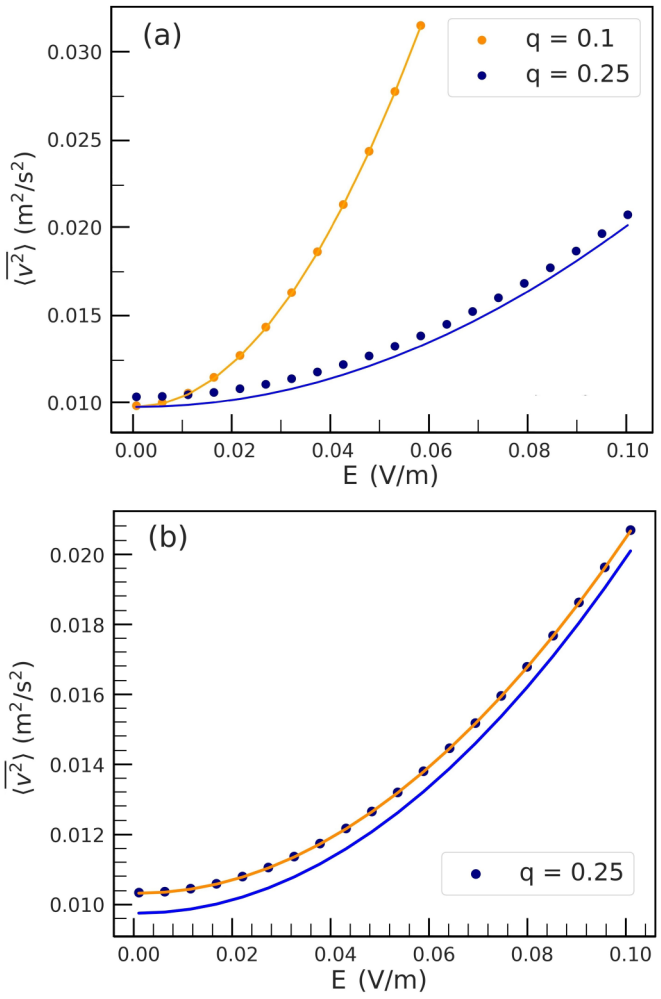

FIG. 3. $\overline{\langle v^2\rangle}$ vs E. Panel (a) shows the dependence for two different values of the q parameter; the points are the numerical results while the solid lines correspond to approximate solutions of Eq. (16). Panel (b) focuses on the $q = 0.25$ case; the solid lines are the fits using Eq. (16) (blue) and Eq. (17) (orange). The rest of the trap parameters are the same as those in Fig. 2 for both panels.

versus the approximation in Eq. (16). As a result, and as expected, we notice that Eq. (16) fails to describe the average square velocity for $q = 0.25$ adequately. Therefore, for a more accurate description of the ion's dynamics, it is necessary to go to the next level of approximation, yielding

$$\overline{\langle x^2\rangle} \approx \left(\frac{k_B T}{m\omega^2} + \frac{\tilde{E}_x^2}{\omega^4}\right)\left[\frac{1 + \frac{27}{50}q^2}{1 - \frac{1}{5}q^2}\right],$$
$$\overline{\langle v^2\rangle} \approx \frac{\Omega^2}{4}\left(\frac{k_B T}{m\omega^2} + \frac{\tilde{E}_x^2}{\omega^4}\right)\left[a\left(\frac{1 + \frac{14}{25}q^2}{1 - \frac{24}{31}q^2}\right) + q^2\left(\frac{1 + \frac{20}{25}q^2}{1 - \frac{7}{50}q^2}\right)\right]$$
$$- \frac{\tilde{E}_x^2}{\omega^2}\left(1 + \frac{q^2}{2}\right), \tag{17}$$

which show a q dependence similar to that in Eq. (16), although a new field-dependent term appears. Equation (17) describes accurately the mean square velocity of the ion for q values as large as 0.25, as it is shown in Fig. 3(b).

Moreover, we notice that higher-order terms of the Fourier expansion for the time-averaged mean square distance with and without excess micromotion are related (see Table I) as

$$x_{n+1,E_{\rm mm}} \approx x_{n+1} + \frac{x_{n+1}}{x_0}\frac{\tilde{E}_x^2}{\omega^4} + S_n^+\left(1+\frac{2\gamma'}{\Omega}i\right)\frac{\tilde{E}_x^2 q}{\Omega^2\omega^2},$$

where x_{n+1} and $x_{n+1,E_{\rm mm}}$ denote the Fourier coefficients in the absence and presence of $E_{\rm mm}$, respectively, and S^+ is given by Eq. (12). Therefore, the contribution of the nth harmonic of the trap frequency depends not only on the q parameter but also on the magnitude of the stray field causing the constant excess micromotion.

Finally, we study a more general scenario including a time-dependent excess micromotion: $\mathrm{F}_{\mathrm{mm}e,x} = e[E_{\mathrm{dc},x} + E_{\mathrm{ac},x}\sin(\Omega t)]$, where $E_{\rm dc}$ is a stray field, as previously considered, and $E_{\rm ac}\sin(\Omega t)$ stands for the new time-dependent component, where the amplitude $E_{\rm ac}$ depends on the trap parameters. The mean position of the ion is found by solving Eq. (8), which leads to

$$\langle x\rangle \approx \left(\frac{\tilde{E}_x}{\omega^2} - \frac{\tilde{E}_x}{\omega^2}e^{\frac{-\gamma' t}{2}}\cos(\omega_d t)\right)\left(1+\frac{q_x}{2}\cos(\Omega t)\right) + \frac{\tilde{E}_{\rm ac}}{\Omega^2}\sin(\Omega t), \tag{18}$$

where $\tilde{E}_{\rm ac} = eE_{\rm ac}/m$, and the mean velocity is obtained upon derivation of Eq. (18) as a function of time. Consequently, the time-averaged values of $\langle x^2\rangle$ and $\langle v^2\rangle$ read as

$$\overline{\langle x^2\rangle} \approx \frac{k_{\rm B}T}{m\omega^2} + \frac{\tilde{E}_{\rm dc}^2}{\omega^4} + \frac{\tilde{E}_{\rm ac}^2}{2\Omega^2\omega^2} - \frac{\tilde{E}_{\rm dc}\tilde{E}_{\rm ac}q\Omega}{16\omega^4\gamma'},$$
$$\overline{\langle v^2\rangle} \approx \frac{2k_{\rm B}T}{m} + \frac{\tilde{E}_{\rm dc}^2}{\omega^2} + \frac{\tilde{E}_{\rm ac}^2}{\Omega^2} - \frac{\tilde{E}_{\rm dc}\tilde{E}_{\rm ac}q\Omega}{8\omega^2\gamma'}, \tag{19}$$

which are different from the case of a constant electric field. In Eq. (19), it is worth emphasizing that the last term coupling the time-dependent component with the time-independent one of stray fields with the Paul trap fields is usually ignored in other derivations [17].

B. Distributions

As a consequence of the time-dependent trapping potential on the ion, the system reaches a quasistationary state rather than a stationary state, in which the trap frequency drives the time evolution. The phase-space distribution for each component in the long-time limit is given by

$$P(x,v,t) = \frac{1}{\sqrt{(2\pi\sigma_{xx})(2\pi\sigma_{vv})(1-\rho_{12}^2)}} \times \exp\left[-\frac{1}{1-\rho_{12}^2}\left(\frac{\delta x^2}{2\sigma_{xx}} - \frac{\rho_{12}\delta x\delta v}{\sqrt{\sigma_{xx}\sigma_{vv}}} + \frac{\delta v^2}{2\sigma_{vv}}\right)\right],$$

where σ_{xx} (σ_{vv}) represents the variance of the position (velocity), δx (δv) is the displacement from the mean value $\langle x\rangle$ ($\langle v\rangle$), and ρ_{12} is the normalized correlation $\frac{\sigma_{xv}}{\sqrt{\sigma_{xx}\sigma_{vv}}}$; all of these parameters are time dependent. Therefore, the time-averaged position distribution reads as

$$\overline{P(x)} = \frac{\Omega}{2\pi}\int_0^{\frac{2\pi}{\Omega}}\int_{-\infty}^{\infty} P(x,v,t)\,dv\,dt = \frac{\Omega}{2\pi}\int_0^{\frac{2\pi}{\Omega}}\frac{dt}{\sqrt{2\pi\sigma_{xx}}}\exp\left[-\frac{\delta x^2}{2(1-\rho_{12}^2)\sigma_{xx}}\left(1-\frac{\sigma_{xv}^2}{\sigma_{vv}}\right)\right], \tag{20}$$

which, unfortunately, cannot be solved analytically. However, an approximate time-averaged distribution can be derived using the average mean square position and velocity from Eqs. (16) and (19) for the cases of time-independent and time-dependent excess of micromotion, respectively. Then, the approximate time-averaged distribution for x is

$$\overline{P(x)} \approx \sqrt{\frac{m\omega^2}{2\pi k_{\rm B}T}}\exp\left[\frac{-m\omega^2\left(x-\frac{\tilde{E}_x}{\omega^2}\right)^2}{2k_{\rm B}T}\right], \tag{21}$$

whereas the approximate velocity distribution becomes

$$\overline{P(v)} \approx \sqrt{\frac{1}{2\pi\left(\frac{2k_{\rm B}T}{m}+\frac{\tilde{E}_x^{\,2}}{\omega^2}\right)}}\exp\left[-\frac{1}{2}\frac{v_x^2}{\left(\frac{2k_{\rm B}T}{m}+\frac{\tilde{E}_x^{\,2}}{\omega^2}\right)}\right]. \tag{22}$$

Since we have used the approximated mean values in Eq. (16), this time-averaged distribution works in the pseudopotential regime. The accuracy of Eqs. (20) and (22) is contrasted in Fig. 4, in which the numerical results for the probability distribution for the ion's position and velocity are shown. As a result, it is observed that the derived approximated expressions perform exceptionally well compared to numerical results.

IV. COLORED NOISE BATH

In the case of a bath with a memory effect, the ion's dynamics is described by the GLE [Eq. (2)]. Hence, the probability distribution $P(x,v,t)$ is no longer Markovian, and its statistical properties depend on the type of noise chosen to characterize the bath. In particular, we consider a Gaussian noise with an exponentially decaying correlation function of the form

$$\langle\zeta_{\rm c}(t)\zeta_{\rm c}(s)\rangle = \frac{D}{\tau_{\rm c}}\exp\left(-\frac{|t-s|}{\tau_{\rm c}}\right), \tag{23}$$

where the strength D and the correlation time ($\tau_{\rm c}$) depend on the atom-ion scattering properties. This noise is described as an Ornstein-Uhlebeck (OU) process as

$$\dot{\zeta_{\rm c}} = -\frac{1}{\tau_{\rm c}}\zeta_{\rm c} + \frac{\sqrt{D}}{\tau_{\rm c}}\zeta, \tag{24}$$

where ζ represents a *white noise*. Then, to elucidate the ion's dynamics, one needs to solve a set of integrodifferential stochastic equations constituted by Eq. (2), including the noise effects through Eq. (24).

A. Correlation time

The correlation time is estimated as the atom-ion collisional time $\tau_{\rm c} = \frac{1}{\Gamma_{\rm L}}$, in which

$$\Gamma_{\rm L} = \rho k_{\rm L},$$

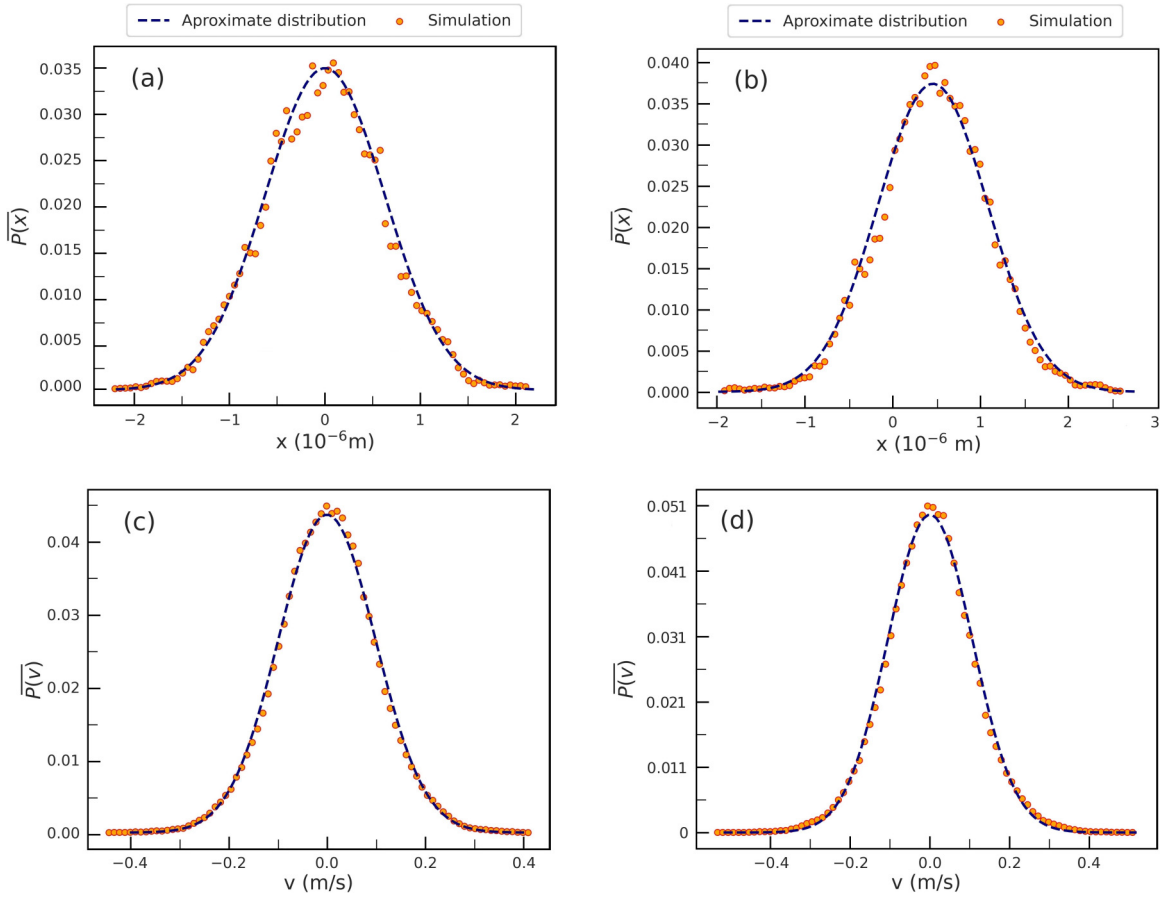

FIG. 4. Probability density function for the ion's position and velocity after solving the Langevin equation. The fitting distributions are the approximate time-averaged distributions previously derived in Eqs. (21) and (22). Panels (a) and (b) present the x-position distribution without a stray field and with a stray field of 0.01 V/m, respectively. Panels (c) and (d) present the v distribution for the same stray field conditions as in panels (a) and (b), respectively. For all the simulations we use the trap parameters $a = -8 \times 10^{-6}$, $q = 0.1$, and $\Omega = 2\pi \times 10^6$ Hz. A total of 1×10^6 points were used for the distributions. Again, a $^{171}Yb^{+}$-^{6}Li mixture was considered in the calculations.

is the Langevin rate for atom-ion collisions, ρ is the density of the bath, and k_L is the Langevin reaction rate given by [4]

$$k_L = 2\pi\sqrt{\frac{C_4}{\mu}},$$

where μ is the atom-ion reduced mass and $C_4 = \alpha/2$ (in atomic units), with α being the polarizability of the atoms from the bath. It is worth noticing that even though the Langevin model for charged-neutral collisions is based on a classical framework, it applies to temperatures as low as 100 μK (depending on the mass of the colliding partners) [23].

B. Ion dynamics

The mean position and the mean velocity are determined in a two-step approach: first Eq. (24) is solved using the stochastic method explained in Appendix B, generating a *colored noise* vector ($\vec{\zeta}_c$). Second, the noise vector is used in the GLE, which is solved using a finite difference method (see Appendix B). In particular, in each run we generate 10^6 realizations to generate average evaluations for any dynamical observable.

Figure 5 displays the evolution of the ion's mean position considering white and colored noises (with two different correlation times). The addition of a new timescale associated with τ_c introduces a delay in the relaxation time of the processes, hindering the evolution into a quasisteady state. Similarly, the colored noise results slightly increase the secular frequency, which can be seen as a retarded effect due to the memory kernel. Moreover, the colored noise induces oscillations in the observables' evolution, even in the case of a simple free Brownian particle [24]: *memory oscillations* are coupled to the secular ones, resulting in a modified secular displacement.

Figure 6 presents the relaxation process of the kinetic energy for white and colored noises. As a result, it can be noticed that the quasistationary behaviors of the two formulations coincide. Thus, the average mean values for colored and white noises are equivalent. Similarly, since the GLE is linear in x, v, and the noise, the phase-space distribution $P(x, v, t)$ will show a shape similar to the one described for the white noise case in Fig. 4. On the other hand, the timescales associated with the friction coefficient and the bath correlations depend on the atomic density. Therefore, by varying the density of the atomic gas, it is possible to tailor the role of memory effects. In particular, for a given

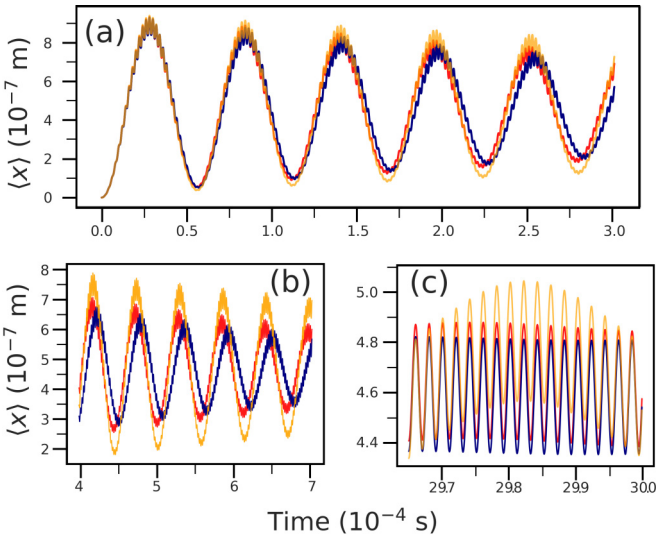

FIG. 5. Expected position for the $^{171}Yb^{+}$ ion in the ^{6}Li cloud using white noise (blue lines) and colored noise with correlation times equal to $\tau = 1.04 \times 10^{-6}$ s (red lines) and $\tau = 1.54 \times 10^{-6}$ s (yellow lines). All the trap parameters are equal for each simulation: $q = 0.1$, $a = -8 \times 10^{-6}$, $\Omega = 2\pi \times 10^{-6}$ Hz, and $E_{mm} = 0.01$ V/m. The panels depict the expected position at different time intervals. Panel (a) represents the evolution from 0 to 300 μs, panel (b) represents the evolution from 400 to 700 μs, and panel (c) shows the behavior between 2.97 and 30.0 ms.

ion, correlation effects increase with the mass-to-polarization ratio of the atom. The simulation in Fig. 4 considers the ion at rest in the center of the trap initially and then goes through a thermalization process with the atomic bath. As shown above, the final time-averaged kinetic energy depends only on the bath temperature, so if the initial condition represents

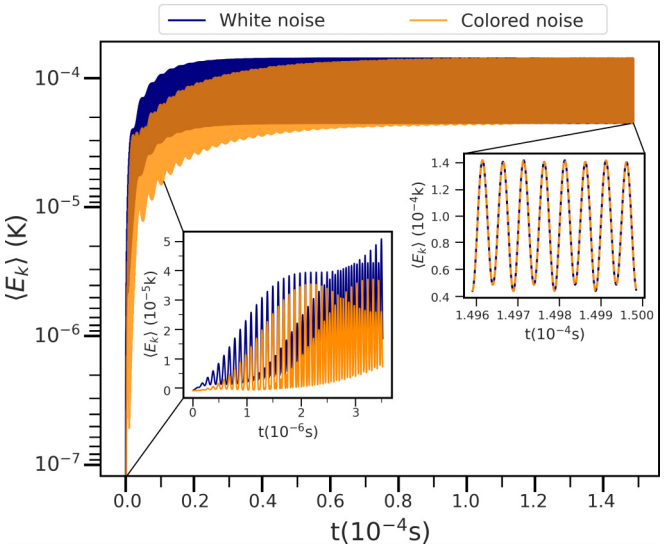

FIG. 6. Energy relaxation for two different noise models in a ^{6}Li-$^{171}Yb^{+}$ system. The agreement of both descriptions, for a given atom-ion mixture, depends of the atomic density. The ion was initially at rest in the center of the trap. However, a different initial condition will converge to the same final energy.

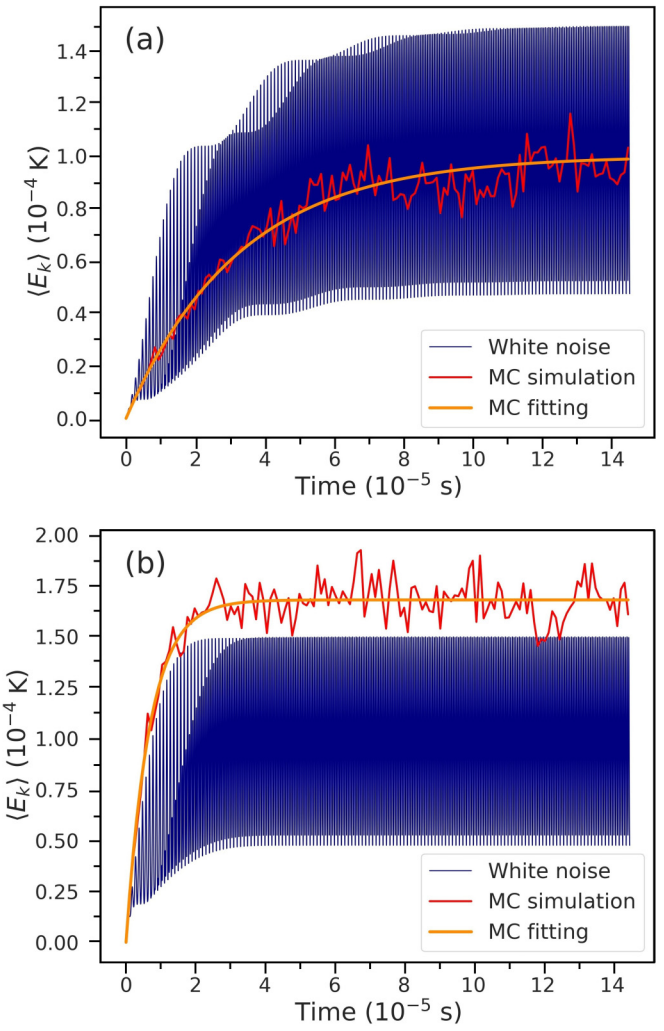

FIG. 7. Average x-contribution kinetic energy as a function of time of a single $^{171}Yb^{+}$ ion immersed in an atomic bath based on MC simulations and on solving the LE with white noise: (a) ^{6}Li and (b) ^{87}Rb.

an excited ion, it will go through a buffer gas cooling process until the same final thermalization state is reached.

V. MONTE CARLO SIMULATIONS

In addition to the Langevin equation formulation, we have also implemented a Monte Carlo simulation of the ion-atom dynamics following Ref. [12]. This simulation works only in the regimen of pseudopotential approximation and assumes that atom-ion collisional cross sections are well described by the Langevin one. We compare the results obtained with this formulation and the stochastic dynamics.

The time evolution of the x-component contribution to the kinetic energy for both white noise Langevin (LE) and Monte Carlo (MC) simulations for two different atomic baths are displayed in Fig. 7. As a result, we notice that the LE simulations show the oscillatory behavior in the energy evolution due to the trapping potential, which has to do with the intrinsic continuous-time nature of the Langevin equation. Nevertheless, the average value of Langevin predictions agrees with

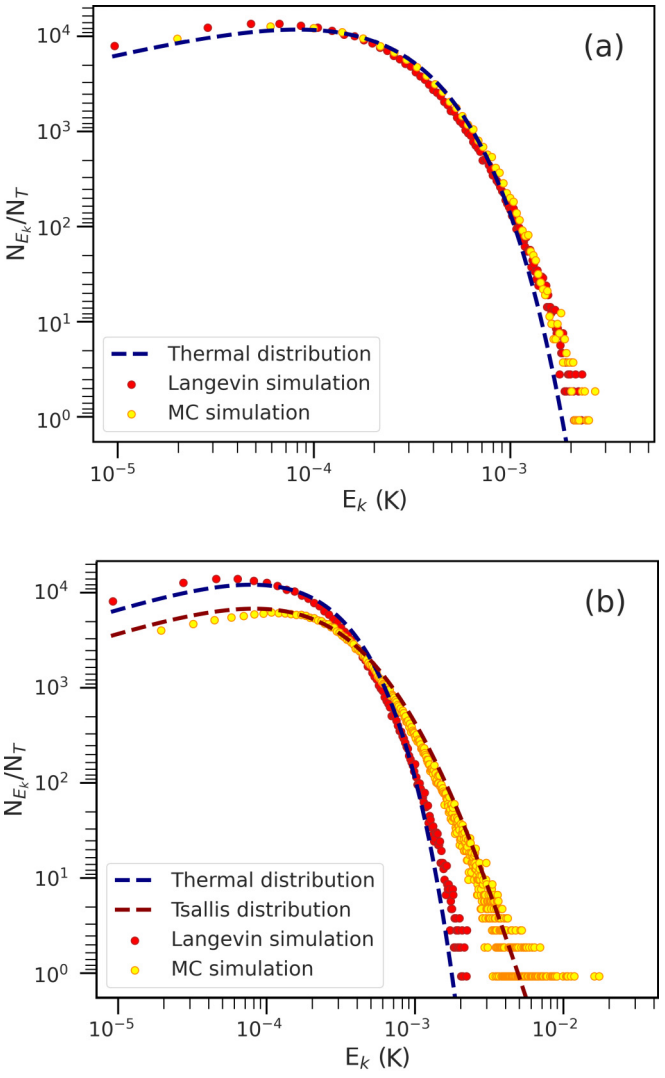

FIG. 8. Kinetic energy distribution of the $^{171}Yb^{+}$ ion in an atomic cloud of (a) ^{6}Li and (b) ^{87}Rb, both at $T = 10^{-4}$ K.

MC simulations in the case of an atomic bath of ^{6}Li. However, there is a discrepancy in the case of ^{87}Rb. Indeed, Langevin's model predictions look almost the same independently of the mass of the atoms in the bath since only the ion mass explicitly appears in the Langevin equation. On the contrary, in MC simulations, the relevant parameter is the atom-ion reduced mass. We extract the relaxation times by fitting the MC results to a time-dependent decaying exponential for a more exhaustive comparison between both simulation approaches. For the ^{6}Li atomic bath, we obtained relaxations times of 23.00 and 22.79 μs for the Langevin and Monte Carlo simulations, respectively, resulting in a relative error of 9.36% between the two schemes. In contrast, the error associated with the average kinetic value for long times is just 0.3%. However, for a ^{87}Rb atomic bath, the relaxation times and the average kinetic energy become very different between both formulations; the associated error for the mean kinetic energy is more significant than 50% and even more prominent for the relaxation times, resulting in a value of 8.16 μs for the Langevin simulation and less than 4 μs for the Monte Carlo scheme.

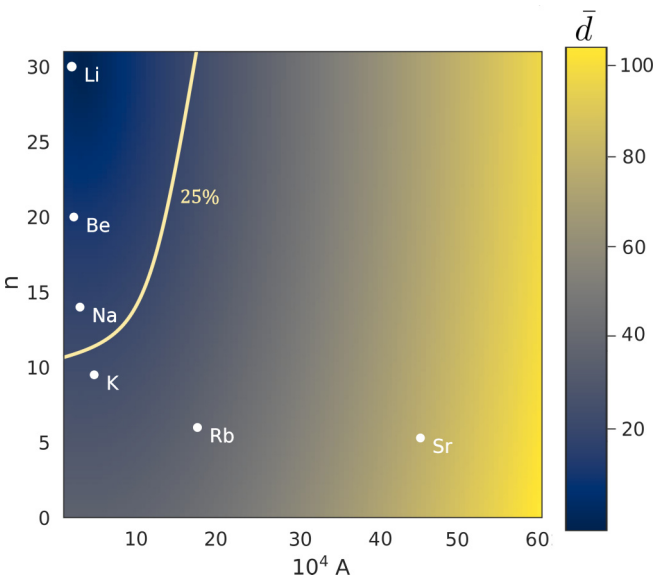

FIG. 9. Validity of the stochastic approach. The two parameters of the Tsallis distribution n and A are represented in the y axis and the x axis, respectively, whereas the color bar represents the average distance ($\bar{d}$) of using the stochastic approach versus the Monte Carlo method. The plotted curve represents a contour at 25% of error that we consider the limiting of the stochastic approach.

Figure 8 presents the kinetic energy distribution of a $^{171}Yb^{+}$ ion immersed in two different baths. For the ^{6}Li bath [Fig. 8(a)], both formulations lead to a thermal distribution characterized for the atomic cloud temperature (T_a), with an ion kinetic temperature of $T_{kin} \approx 3T_a/5$. On the other hand, MC simulations for the ^{87}Rb bath [Fig. 8(b)] reveal a different behavior: the kinetic energy distribution follows a Tsallis distribution of the form [25]

$$P(E_k) = A\frac{(n-2)(n-3)(n-4)}{2(nk_BT)^3}\frac{E_k^{1/2}}{\left(1+\frac{E_k}{nk_BT}\right)^n}, \qquad (25)$$

where A, n, and T are fitting parameters that for the case at hand are 1.2×10^{-4}, 6.0, and 7×10^{-4} K, respectively. The parameter T represents the physical temperature in the limit of the thermal distribution ($n \to \infty$). This power-law behavior is a result of the so-called *micromotion heating* and depends strongly on the atom-to-ion mass ratio and the trap parameters [25]. However, the stochastic formulation still leads to a thermal distribution due to the noise statistics and the additive nature of the stochastic equation of motion. Therefore, these results indicate that stochastic formulations for describing the ion dynamics in a bath are only applicable in the regimen of a low atom-to-ion mass ratio at which the heating effects are almost negligible but not null, as observed in Fig. 8.

In order to establish a validity region for the stochastic formulation, we have performed MC simulations for atom-ion collisions in a wide range of ion-to-atom mass ratios. The resulting energy distributions have been fitted with a Tsallis distribution, keeping T as the physical temperature for different atoms and the same ion Yb^{+}. Then, considering that Li behaves thermally, it is possible to analyze different atoms by looking into the average distance of the (A, n) vector concerning Li, labeled as $\bar{d}$, as shown in Fig. 9. As a result,

assuming that the stochastic approach is appropriate up to $\bar{d} \lesssim 25\%$, we can conclude that atoms lighter than Na mass in the presence of a Yb^+ ion are adequately described by the stochastic approach.

VI. CONCLUSIONS

We have studied the dynamics of a single trapped ion in a bath of ultracold atoms via the Langevin equation. The bath induces a stochastic force whose amplitude is controlled by atom-ion scattering properties. In addition, we have obtained analytical solutions for the average mean square position and the kinetic energy of the ion up to values $q \leqslant 0.3$. Similarly, the present formulation allows us to study the impact of excess micromotion (time-dependent and time-independent), leading to analytical expressions for relevant magnitudes. In particular, we find that the excess micromotion adds energy to the system because of the time-varying trap potential. Moreover, we have derived an approximated position and velocity distribution for the ion with excess micromotion within the pseudopotential regimen. As a result, it is possible to estimate any necessary time-dependent or average property of the system.

The effects of the bath nature on the ion dynamics have been studied, comparing results from a white noise bath versus a colored noise bath. In particular, we have noticed that a colored noise bath requires solving the generalized Langevin equation. Therefore, it entails more physical information on the atom-ion few-body physics. In particular, the correlation time of the colored noise plays an essential role in the relaxation timescale of the ion. Although, those effects are mitigated by choosing an atomic species with a low mass-to-polarization ratio.

Finally, the results of the stochastic formulation have been tested against Monte Carlo simulations. The two formulations describe similar energy evolutions and distributions in the low atom-to-ion mass ratio regimen, where the *micromotion heating* reduces its contribution. The stochastic formulation turns out to be computationally cheaper than Monte Carlo simulations. For instance, 10^5 collision events for ^{6}Li-$^{171}Yb^+$, with $n = 2 \times 10^{20}$ m^{-3}, takes a CPU time of 461.66 s, whereas it takes 331.46 s for the Langevin simulation. This difference increases linearly with the simulation time for the time range required to have stable averages. Additionally, it offers the possibility to explore the spectral aspects of the time evolution or the consideration of any bath correlation, which can be associated with the physical characteristics of the bath.

ACKNOWLEDGMENT

J.M. acknowledges support from the Universidad del Valle (Grant No. CI 71212).

APPENDIX A: ION-ATOM FEW-BODY PHYSICS

The diffusion cross section is given by [26]

$$\sigma_{\rm D}(E_k) = \int \frac{d\sigma_{\rm el}(E_k)}{d\Omega}(1-\cos\theta)d\Omega, \tag{A1}$$

where $\frac{d\sigma_{\rm el}(E_k)}{d\Omega}$ represents the elastic differential cross section either classical or quantal, $d\Omega = 2\pi \sin\theta d\theta$ is the solid angle element, and θ is the scattering angle. Assuming a quantum mechanical description of the scattering observables, Eq. (A1) can be written as [26]

$$\sigma_{\rm D}(E_k) = \frac{4\pi}{k^2}\sum_{l=0}^{\infty}(l+1)\sin^2\left[\delta_{l+1}(E_k) - \delta_l(E_k)\right], \tag{A2}$$

where $\delta_l(E_k)$ is the phase shift for a given partial wave l and collision energy E_k.

In this work, the phase shifts for $^{174}Yb^+$-Li and $^{174}Yb^+$-Rb collisions from 1 μK to 1 K have been calculated using a single-channel description of the scattering. In particular, the Numerov method is employed to propagate the wave function from a distance between $4.8\,a_0$ and $12\,000\,a_0$ with a step size of $0.006\,a_0$ for $^{174}Yb^+$-Li, whereas for $^{174}Yb^+$-Rb the propagation took place between $5.8\,a_0$ and $15\,000\,a_0$ with a step size of $0.003\,a_0$. The number of partial waves included varied with the collision energy, but we included as many as necessary to ensure a convergence better than 1% of the elastic cross section.

Scattering properties at low collision energies are mainly dominated by the long-range tail of the atom-ion interaction potential. Therefore, we employ atom-ion potentials with the physical long-range part but with an artificial short-range part. In particular for $^{174}Yb^+$-Li the potential reads

$$V(r) = \frac{C_6}{r^6} - \frac{C_4}{r^4}, \tag{A3}$$

with $C_4 = 82$ a.u. and $C_6 = 29284$ a.u. The same potential has been used previously in quasiclassical trajectory calculations showing that the short-range part of the atom-ion interactions has a negligible impact on scattering observables in the cold regime [27,28]. Whereas, for $^{174}Yb^+$-Rb the potential is taken as

$$V(r) = -\frac{C_4}{r^4}\left[1 - \frac{1}{2}\left(\frac{r_m}{r}\right)^4\right], \tag{A4}$$

with $C_4 = 160$ and $r_m = 10.142\,a_0$ corresponding to the $a^3\Sigma$ state.

APPENDIX B: NUMERICAL SOLUTION OF THE GENERALIZED LANGEVIN EQUATION

The description of the generalized Langevin dynamics of the ion in a bath requires one to solve a set of stochastic integrodifferential equations including Eq. (2) and the equation associated with the generation of the noise. For the OU noise considered here the equations are

$$\frac{d^2x}{dt^2} + \int_0^t \frac{\Gamma(t-t')}{m}v(t')dt' + \frac{\Omega_{\rm RF}^2}{4}[a + 2q\cos(\Omega_{\rm RF}t)]x = F_x, \tag{B1}$$

$$\frac{dx}{dt} = v, \tag{B2}$$

$$\frac{d\zeta_c}{dt} = -\frac{1}{\tau_c}\zeta_c + \frac{\sqrt{D}}{\tau_c}\zeta, \tag{B3}$$

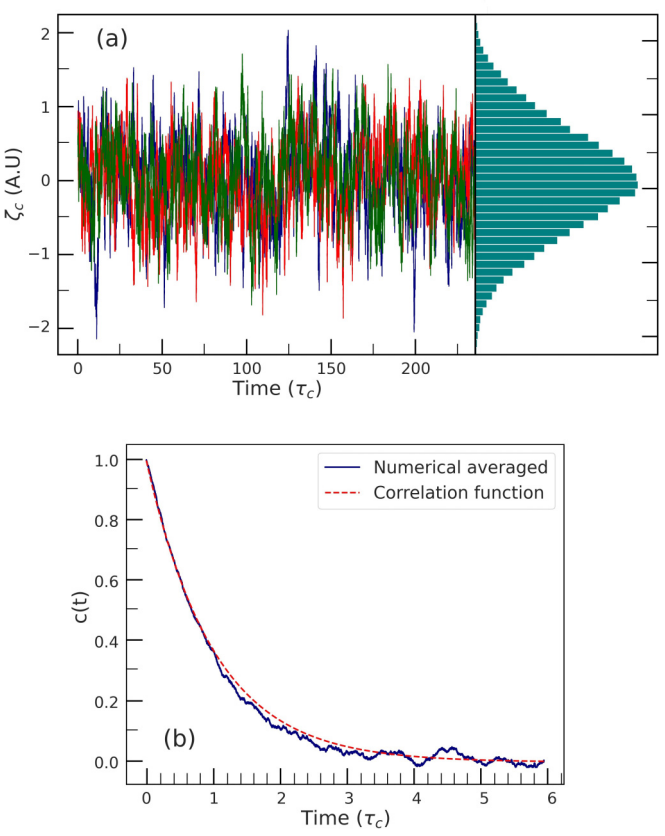

FIG. 10. Colored noise resulting from solving the OU equation (B3). Panel (a) shows three different realizations of the OU noise and its distribution, and panel (b) displays the correlation function of the noise fitting with Eq. (23).

where $F_x = \tilde{E}_x + \zeta_c(t)$. The third equation is the OU process, $\zeta_c(t)$ refers to the generated colored noise and $\zeta(t)$ is the driver white noise. To solve numerically this set of equations, we first solve the independent OU equation (B3) using a stochastic finite difference scheme to generate a colored noise vector in the time grid. This noise vector is implemented in the solution of the two first coupled equations, Eqs. (B1) and (B2).

The finite difference scheme for the solution of Eq. (B3) is based on the method proposed in Ref. [29]. The colored noise for each iteration is given by

$$\zeta_{c\,i+1} = \left(1 - \frac{\Delta t}{\tau_c}\right)\zeta_{c\,i} + \frac{\sqrt{D}}{\tau_c} w(0,1)\sqrt{\Delta t},$$

where Δt is the time step and $w(0,1) \sim N(0,1)$ is a Gaussian random variable with a mean of 0 and a standard deviation equal to 1. The results are shown in Fig. 10, where different realizations of the colored noise and its correlation function are displayed.

Next, the solutions ζ_{ci} are used in the two coupled differential equations, Eqs. (B1) and (B2), for r_i and v_i, which are solved using the following finite difference representation:

$$x_{i+1} = \left[2 - \frac{\Omega^2}{4}[a + 2q\cos(\Omega_{RF}t)]\Delta t^2\right]x_i - x_{i-1} + \left[\tilde{E}_x + \frac{\zeta_c(t)}{m} - S_i\right]\Delta t^2,$$

where $S_i = S(t_i)$ is the integral term in Eq. (2). The correlation function and the fluctuation-dissipation relation allow us to express the integral in a recursive form as

$$S_{i+1} = S_i + \frac{1}{2k_B T}\left[\exp\left(\frac{\Delta t}{\tau_c}\right)v_{i+1} + v_i\right].$$

Finally, the velocity vector is obtained using central differences. The procedure is repeated for several realizations N_{int} ($\sim 10^6$), and then the statistical average of the quantity (position or velocity) is computed to obtain its mean value.

In the case of a white noise, the Langevin dynamics is obtained after solving only Eq. (7) using a finite difference scheme, yielding

$$x_{i+1} = \frac{\left(\frac{\gamma'\Delta t}{2} - 1\right)x_{i-1} - \left(\frac{\Omega^2}{4}[a + 2q\cos(\Omega t)]\Delta t^2 - 2\right)x_i + \left(\tilde{E}_x + \frac{\sqrt{D}w(0,1)}{m}\right)\Delta t^2}{1 + \frac{\gamma'\Delta t}{2}},$$

and the velocity is computed from central differences.

The timescales associated with the Langevin dynamics of the ion are the Paul trap period ($T_{RF} = 2\pi/\Omega$), the relaxation time regarding the friction ($\tau_R = 1/\gamma'$), and the correlation time (τ_c) for the case of colored noise. For the atomic densities and bath temperatures considered in our calculations, τ_R and τ_c are $\gtrsim 2 \times 10^{-6}$ s. Then the short time involved comes from the trap period ($T_{RF} \leqslant 1 \times 10^{-6}$ s). Then, for the numerical solution, we fix a time interval of $\Delta t = 5 \times 10^{-9}$ s which allows us to compute several steps within the same RF oscillation.

APPENDIX C: RADIAL DISTRIBUTION FUNCTION

Using the approximate position distribution for the x and y components we find the radial distribution as

$$\overline{P(r)} \propto {}_0\tilde{F}_1\left(;1;\frac{\tilde{E}_x^2 r^2}{\omega^4}\right) r \exp\left(\frac{-m\omega^2 r^2}{2k_B T}\right) \xrightarrow[E_x=0]{} \approx \frac{m\omega^2}{k_B T} r \exp\left(\frac{-m\omega^2 r^2}{2k_B T}\right), \tag{C1}$$

where ${}_0\tilde{F}_1(;1;\frac{\tilde{E}_x^2 r^2}{\omega^4})$ is the regularized hypergeometric function defined as

$$ {}_0\tilde{F}_1\left(;1;\frac{\tilde{E}_x^2 r^2}{\omega^4}\right) = \frac{1}{2\pi}\int_0^{2\pi} \exp\left(\frac{2\tilde{E}_x r}{\omega^2}[\cos(\theta)+\sin(\theta)]\right)d\theta. $$

In addition, the stationary distribution for the harmonic z component is simply given by

$$ P(z) = \sqrt{\frac{m\omega_z^2}{2\pi k_B T}} \exp\left[\frac{-m\omega_z^2 z^2}{2k_B T}\right], \tag{C2} $$

where $\omega_z^2 = \frac{\Omega_{RF}^2}{4} a_z$.

Finally, $\overline{P(r)}$ and $P(z)$ give an idea of the averaged 3D ion position distribution in the trap. Figure 11 shows the performance of the approximate radial distribution versus the numerical one. In the absence of excess micromotion, the regularized hypergeometric function equals 1. As a result, the distribution is identical to the radial distribution for a particle in the harmonic pseudopotential:

$$ \left[\frac{a\Omega^2}{4} + \frac{q^2\Omega^2}{4}\right] \approx 2\omega. \tag{C3} $$

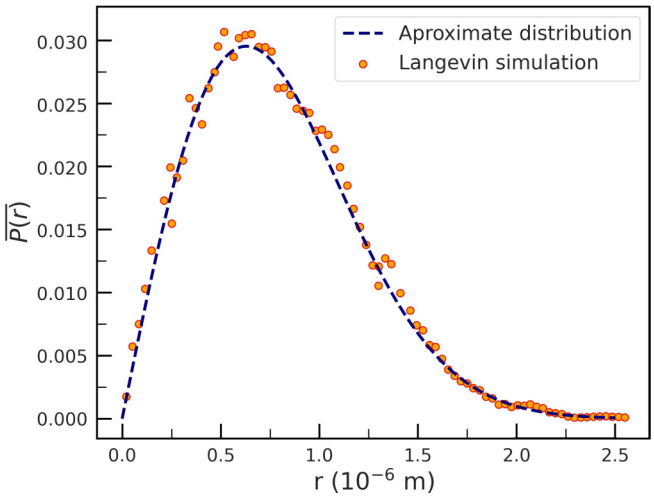

FIG. 11. Radial distribution of the ion fitting by the approximate distribution (C1). To achieve an accurate fitting the trap parameters are the same as those in Fig. 4.

[1] W. M. Itano, J. C. Bergquist, J. J. Bollinger, and D. J. Wineland, Cooling methods in ion traps, Phys. Scr. **T59**, 106 (1995).

[2] W. W. Smith, O. P. Makarov, and J. Lin, Cold ion-neutral collisions in a hybrid trap, J. Mod. Opt. **52**, 2253 (2005).

[3] M. Tomza, K. Jachymski, R. Gerritsma, A. Negretti, T. Calarco, Z. Idziaszek, and P. S. Julienne, Cold hybrid ion-atom systems, Rev. Mod. Phys. **91**, 035001 (2019).

[4] J. P. Ríos, *An Introduction to Cold and Ultracold Chemistry: Atoms, Molecules, Ions and Rydbergs* (Springer, Berlin, 2020).

[5] J. M. Schurer, P. Schmelcher, and A. Negretti, Ground-state properties of ultracold trapped bosons with an immersed ionic impurity, Phys. Rev. A **90**, 033601 (2014).

[6] P. Massignan, C. J. Pethick, and H. Smith, Static properties of positive ions in atomic Bose-Einstein condensates, Phys. Rev. A **71**, 023606 (2005).

[7] J. Pérez-Ríos, Cold chemistry: a few-body perspective on impurity physics of a single ion in an ultracold bath, Mol. Phys. **119**, e1881637 (2021).

[8] C. C. Bradley, C. A. Sackett, J. J. Tollett, and R. G. Hulet, Evidence of Bose-Einstein Condensation in an Atomic Gas with Attractive Interactions, Phys. Rev. Lett. **75**, 1687 (1995).

[9] F. Schreck, L. Khaykovich, K. L. Corwin, G. Ferrari, T. Bourdel, J. Cubizolles, and C. Salomon, Quasipure Bose-Einstein Condensate Immersed in a Fermi Sea, Phys. Rev. Lett. **87**, 080403 (2001).

[10] F. G. Major and H. G. Dehmelt, Exchange-collision technique for the rf spectroscopy of stored ions, Phys. Rev. **170**, 91 (1968).

[11] M. Cetina, A. T. Grier, and V. Vuletić, Micromotion-Induced Limit to Atom-Ion Sympathetic Cooling in Paul Traps, Phys. Rev. Lett. **109**, 253201 (2012).

[12] C. Zipkes, L. Ratschbacher, C. Sias, and M. Köhl, Kinetics of a single trapped ion in an ultracold buffer gas, New J. Phys. **13**, 053020 (2010).

[13] H. Fürst, N. Ewald, T. Secker, J. Joger, T. Feldker, and R. Gerritsma, Prospects of reaching the quantum regime in Li-Yb^+ mixtures, J. Phys. B: At., Mol. Opt. Phys. **51**, 195001 (2018).

[14] J. Joger, H. Fürst, N. Ewald, T. Feldker, M. Tomza, and R. Gerritsma, Observation of collisions between cold li atoms and Yb^+ ions, Phys. Rev. A **96**, 030703(R) (2017).

[15] S. Bellaouini, A. Pal, A. Rakshit, M. Farjallah, B. Deb, and H. Berriche, Structure, spectroscopy and cold collisions of the $(SrNa)^+$ ionic system, Eur. Phys. J. D **72**, 131 (2018).

[16] R. Saito, S. Haze, M. Sasakawa, R. Nakai, M. Raoult, H. Da Silva, O. Dulieu, and T. Mukaiyama, Characterization of charge-exchange collisions between ultracold ^{6}Li atoms and $^{40}Ca^+$ ions, Phys. Rev. A **95**, 032709 (2017).

[17] D. J. Berkeland, J. D. Miller, J. C. Bergquist, W. M. Itano, and D. J. Wineland, Minimization of ion micromotion in a Paul trap, J. Appl. Phys. **83**, 5025 (1998).

[18] H. Dehmelt, Radiofrequency spectroscopy of stored ions I: Storage, Adv. At. Mol. Phys. **3**, 53 (1968).

[19] It is worth noticing that even in the presence of an external field, the fluctuation-dissipation theorem holds since the external field only affects the Brownian particle.

[20] R. J. O. Hirschfelder, C. F. Curtiss, and R. B. Bird, *Molecular Theory of Gases and Liquids* (Wiley, New York, 1954).

[21] Note that in a linear Paul trap the dynamics in each coordinate are independent of each other.

[22] R. Blatt, P. Zoller, G. Holzmüller, and I. Siemers, Brownian motion of a parametric oscillator: A model for ion confinement in radio frequency traps, Z. Phys. D: At., Mol. Clusters **4**, 121 (1986).

[23] R. Côté and A. Dalgarno, Ultracold atom-ion collisions, Phys. Rev. A **62**, 012709 (2000).

[24] J. Schmidt, A. Meistrenko, H. van Hees, Z. Xu, and C. Greiner, Simulation of stationary Gaussian noise with regard to the Langevin equation with memory effect, Phys. Rev. E **91**, 032125 (2015).

[25] M. Pinkas, Z. Meir, T. Sikorsky, R. Ben Shlomi, N. Akerman, and R. Ozeri, Effect of ion-trap parameters on energy distributions of ultra-cold atom-ion mixtures, New J. Phys. **22**013047 (2020).

[26] N. F. Mott and S. W. Massey, *The Theory of Atomic Collisions* (Oxford University, Oxford, England, 1965).

[27] H. Hirzler, E. Trimby, R. S. Lous, G. C. Groenenboom, R. Gerritsma, and J. Pérez-Ríos, Controlling the nature of a charged impurity in a bath of Feshbach dimers, Phys. Rev. Research **2**, 033232 (2020).

[28] H. Hirzler, R. S. Lous, E. Trimby, J. Pérez-Ríos, A. Safavi-Naini, and R. Gerritsma, Observation of Chemical Reactions between a Trapped Ion and Ultracold Feshbach Dimers, Phys. Rev. Lett. **128**, 103401 (2022).

[29] G. Volpe and G. Volpe, Simulation of a brownian particle in an optical trap, Am. J. Phys. **81**, 224 (2013).